Journal of Dentistry 81 (2019) 70–84

Contents lists available at ScienceDirect

Journal of Dentistry

journal homepage: www.elsevier.com/locate/jdent

Nanoparticles having amphiphilic silane containing Chlorin e6 with strong anti-biofilm activity against periodontitis-related pathogens

Xiaolin Sun[a], Lin Wang[a,*], Christopher D. Lynch[b], Xueke Sun[c], Xue Li[a], Manlin Qi[a], Cui Ma[d], Chunyan Li[a], Biao Dong[c,*], Yanmin Zhou[a,*], Hockin H.K. Xu[e,f,g]

[a] Department of Oral Implantology, School of Stomatology, Jilin University, Changchun, 130021, China
[b] Restorative Dentistry, University Dental School and Hospital, University College Cork, Wilton, Cork, Ireland
[c] State Key Laboratory on Integrated Optoelectronics, College of Electronic Science and Engineering, Jilin University, Changchun, 130012, China
[d] Department of Pediatric Hematology, First Hospital, Jilin University, Changchun, 130021, China
[e] Department of Advanced Oral Sciences and Therapeutics, University of Maryland School of Dentistry, Baltimore, MD, 21201, USA
[f] Center for Stem Cell Biology & Regenerative Medicine, University of Maryland School of Medicine, Baltimore, MD, 21201, USA
[g] Marlene and Stewart Greenebaum Cancer Center, University of Maryland School of Medicine, Baltimore, MD, 21201, USA

ARTICLE INFO

Keywords:
Photodynamic therapy
Photosensitizer
Amphiphilic silane
Periodontitis
Antibacterial
Magnetic targeting

ABSTRACT

Objectives: The objectives of this study were to: (1) develop the multifunctional nanoparticles containing Chlorin e6 (Ce6), Coumarin 6 (C6) and Fe_3O_4 nanoparticles (NPs); and (2) investigate the inhibitory effects of the nanoparticles via antibacterial photodynamic therapy (aPDT) against three species of periodontitis-related pathogens for the first time.

Materials and methods: Ce6 and C6 were co-loaded into the Fe_3O_4-silane core-shell structure to form multifunctional nanoparticles (denoted "Fe_3O_4-silane@Ce6/C6 MNPs"). The physical and chemical properties of nanoparticles were characterized. Biofilm properties of *Streptococcus sanguinis*, *Porphyromonas gingivalis* and *Fusobacterium nucleatum* were tested. Colony-forming units (CFU), live/dead assay, and metabolic activity of biofilms were determined to evaluate the aPDT function mediated by the Fe_3O_4-silane@Ce6/C6 MNPs. Fluorescence imaging and the targeted antibacterial effects were also investigated.

Results: Fe_3O_4-silane@Ce6/C6 MNPs showed superparamagnetic properties, chemical stability and water-solubility, with no cytotoxicity. Fe_3O_4 NPs did not compromise the emission peaks of C6 and Ce6. The Fe_3O_4-silane@Ce6/C6-mediated aPDT had much greater reduction in biofilms than the control groups ($p < 0.05$). Biofilm CFU was reduced by about 4–5 orders of magnitude via Fe_3O_4-silane@Ce6/C6-mediated aPDT. The co-loading of Ce6 and C6 enabled the real-time aPDT monitoring by ratio emissions with the same wavelength. Fe_3O_4 with magnetic field enabled the targeting of infection sites by killing bacteria via magnetic field.

Conclusion: The multifunctional nanoparticles exerted strong anti-biofilm activity against periodontitis-related pathogens, with excellent biocompatibility, real-time monitoring, and magnetically-targeting capacities. The multifunctional nanoparticles have great potential in antibacterial applications to inhibit the occurrence and progression of periodontitis.

1. Introduction

Periodontitis is a common chronic inflammatory disease leading to alveolar bone resorption and tooth loss. The prevalence of periodontitis is reported by European and United States studies to range from 31% to 76% [1]. Severe forms of this disease affect 11% of the global population [2]. Periodontitis is mainly caused by oral biofilms which were composed of pathogenic bacterial species. Traditionally, periodontal treatment has involved mechanical debridement to remove the adherence to the infected root surfaces of biofilm and calculus. In addition, adjunctive local antibiotics were administered to eradicate or reduce the number of pathogenic bacteria in periodontal pockets or at the biofilm-gingival interface [3]. However, mechanical debridement fails to remove periodontal infection in a subset of cases without the ability to approach deep pockets, furcation and surface irregularities areas [4,5]. Moreover, there is increasing attention about the abuse of antibiotics in periodontitis treatment due to the world's public health concern for bacterial resistance. Therefore, new alternative strategies

* Corresponding authors.
E-mail addresses: wanglin1982@jlu.edu.cn (L. Wang), dongb@jlu.edu.cn (B. Dong), zhouym62@126.com (Y. Zhou).

https://doi.org/10.1016/j.jdent.2018.12.011
Received 3 October 2018; Received in revised form 12 December 2018; Accepted 18 December 2018

are needed to control plaque and treat periodontal diseases.

Antimicrobial photodynamic therapy (aPDT) is a promising antibacterial therapeutic modality to eliminate the aforementioned shortcomings [6]. Antibacterial PDT, which employs appropriate excitation light in combination with photosensitizers (PS) and oxygen, allows nonspecific attack against microorganisms by generating cytotoxic reactive oxygen species (ROS), especially singlet oxygen ($^1O_2$) [7]. Numerous studies indicated that periodontal bacteria are susceptible to aPDT in planktonic cultures and biofilms [6,8]. In the early 1990s, an attempt was made to employ the redox properties of Methylene blue (MB) for the reduction of bacteria in periodontitis patients [9]. Since then, increasing efforts were made to investigate the clinical effect of aPDT via various PS agents on periodontitis [6,10]. Among them, Chlorin e6 (Ce6) was a promising PS agent with a high sensitizing efficacy, low toxicity and rapid elimination from the body [10]. For in vitro periodontal pathogens, Ce6 also demonstrated high killing activities [11]. However, aPDT had a minimal effect on the viability of microorganisms organized in a bacterial biofilm [12], which was probably due to the hydrophobic nature of the most PS molecules, leading to the reduced penetration of the PS into the biofilm matrix [13]. Nanoparticles (NPs) had been widely developed and applied in the field of dentistry [14,15]. Recently, nanoparticles such as PLGA [16], chitosan [17] and cyclodextrins [18] have been also applied as carriers to deliver PS agents into microorganisms and improve the antimicrobial performance.

A major disadvantage of traditional nanoparticles carrying PS agents is the low delivery efficiency due to the drainage of gingival crevicular fluid and high saliva fluid turnover. PS carriers conjugated with specific antibody were developed to enhance the targeting efficacy of PS, such as epithelial cell-targeting nanoparticles which could target specific lesion tissues and keep a sustained and effective drug concentration in the lesions [19]. However, problems still remain, including interpatient variation in receptor expressions and species differences between the bacteria. Therefore, there is a major need to enhance the delivery and permeability of the PS agent to the exact infected site. In the present study, superparamagnetic iron oxide nanoparticle (IONP)-based PS carriers were designed and used in magnetic field-navigated antibacterial applications.

Real-time monitoring of the drug consumption and distribution is another challenge that should be addressed in periodontitis treatment. The unknown effective dose of therapeutic agents reaching the disease sites is a major uncertainty toward accurate medicine, and usually results in either inadequate doses or overdose during therapy [20]. Dye Coumarin 6 (C6) is a hydrophobic organic molecule which is not sensitive to red light (630 nm wavelength) but can be co-excited with Ce6 by the 405 nm wavelength. Therefore, the Ce6/C6 co-loading method could visually monitor the imaging by measuring the ratio of the metric fluorescence of Ce6/C6. However, to date, there has been no report on nanoparticles containing Ce6/C6 simultaneously and possessing cell-targeting, biocompatibility and real-time aPDT-monitoring functions.

Therefore, the objectives of this study were to: (1) develop antibacterial multifunctional nanoparticles (MNPs) to mediate aPDT for periodontal therapy; and (2) investigate the inhibition efficacy on planktonic bacteria and biofilms of periodontitis-related pathogens for the first time. The following hypotheses were tested: (1) The silane modification would make the nanoparticles stable and biocompatible without cytotoxicity; (2) The aPDT-mediation by multifunctional nanoparticles containing Ce6 would possess much greater killing efficacy than control group; (3) The aPDT effect of Ce6 could be real-time monitored by the ratio metric fluorescence of Ce6/C6; (4) Incorporation of Fe_3O_4 into the nanoparticles would not affect the PDT efficiency while enabling a magnetically-targeting function in periodontitis treatment.

2. Materials and methods

2.1. Synthesis of Fe_3O_4-silane core-shell MNPs with C6 and Ce6

Iron oxide nanoparticles were developed via co-precipitation using $FeCl_3{\cdot}6H_2O$ (Beijing Chemical Works, Beijing, China), $FeCl_3{\cdot}4H_2O$ (Beijing Chemical Works) and an ammonium hydroxide solution under a flow of nitrogen [21]. The mixture of as-prepared Fe_3O_4 nanoparticles and oleic acid (OA, Aladdin, Shanghai, China) were heated to 80 °C with N_2 protection for 30 min. The NPs were mixed in tetrahydrofuran (THF, Beijing Chemical Works) with ultrasonic shaking for 30 min: The OA-Fe_3O_4 NPs (5 mg/mL, 200 μL), Chlorin e6 (Ce6, 3 mg/mL, 300 μL, J&K Scientific Ltd., Beijing, China), Coumarin 6 (C6, 1 mg/mL, 20 μL, J&K Scientific Ltd.) and trimethoxy (octadecyl) silane (7.5 mg/mL, 600 μL, Sigma-Aldrich, St. Louis, MO, USA). Then the solution was rapidly mixed into 5 times the volume of water (pH = 9) for the hydrolyzing process with ultrasonic shaking for 1 min and standing for 3 h. Subsequently, the obtained sample was dialyzed overnight to remove the excess THF. The final product with the core-shell structure was denoted Fe_3O_4-silane@Ce6/C6.

2.2. Characterization of multifunctional nanoparticles

The morphology and size of the multifunctional nanoparticles were characterized by transmission electron microscopy (TEM) and high-resolution TEM (HRTEM) (Electron Microscope FEG-VP Supra 35, Carl Zeiss, Jena, Germany). The Zeta potential and size distribution of the nanoparticles were determined using Zeta potential instrument (Zetasizer, Nano-Z, Malvern Instruments Limited, UK) and dynamic light scattering (DLS). Magnetization hysteresis loops of Fe_3O_4-silane@Ce6/C6 MNPs were recorded by a quantum design superconducting quantum interference device (MPMS-XL7 Magnetometer, Quantum Design, USA). The crystalline structure of samples was measured by X-ray diffraction (XRD) (Diffractometer Rigaku DMax-2000PC, Rigaku Corporation, Tokyo, Japan). UV − vis absorption spectra examinations were performed in 200–600 nm wavelength range using a Shimadzu UV-2550 spectrophotometer (Shimadzu Corporation, Tokyo, Japan). The dispersibility of Fe_3O_4-silane@Ce6/C6 and silane@Ce6/C6 MNPs was measured in water, neutral phosphate buffered saline (PBS, pH = 7.4), acid solution (pH = 4.5) and alkaline solution (pH = 8.0).

2.3. Measurement of singlet oxygen generation

To detect singlet oxygen generation of Fe_3O_4-silane@Ce6/C6 MNPs, fluorescent probe experiments were carried out with 2,2′-bis(anthracene-9,10-diylbis(methylene))-dimalonic acid (ABDA, J&K Scientific Ltd.). The mixture of ABDA (10 ppm) and Fe_3O_4-silane@Ce6/C6 MNPs were exposed to the red-light irradiation (630 nm). The $^1O_2$ generation were determined by recording the reduction of ABDA absorbance that was caused by photobleaching of ABDA.

2.4. Dark cytotoxicity of nanoparticle with Ce6/C6

L929 mouse fibroblast cells were obtained from the Institute of Biochemistry and Cell Biology, the Chinese Academy of Sciences (Shanghai, China) and approved for using by the Institution Review Board of Jilin University School of Dentistry. The fibroblasts were maintained in DMEM medium (HyClone, Logan, UT, USA) supplemented with 1% antibiotics (100 U/mL penicillin and 100 g/mL streptomycin) and 10% fetal bovine serum (Gibco, Carlsbad, CA, USA). Cells were incubated at 37 °C in a humid 5% CO_2 atmosphere.

For the dark cytotoxicity of Fe_3O_4-silane@Ce6/C6 and silane@Ce6/C6 MNPs, L929 cells were incubated in 96-well plate at a density 5000 cells per well for 24 h [22]. Then the cells were incubated with different concentration of Fe_3O_4-silane@Ce6/C6 and silane@Ce6/C6 MNPs for another 24 h in dark. The cell viability was determined by CCK-8 (7sea

biotech, China) following the instructions. Wells without any nanoparticles served as calibrators [22]. The percentage survival was calculated and based on the control sample without any treatment as being 100%. All measurements were tested in three replicates.

L929 cells were incubated in a 24-well plate at 37 °C for 24 h [22]. Then the cells were treated with the Ce6 weight concentration of 2.5 μM, 5 μM and 10 μM of Fe_3O_4-silane@Ce6/C6 and silane@Ce6/C6 MNPs for another 24 h. Cells without nanoparticles were used as control. 4% paraformaldehyde was applied to fix the cell, followed by washing with PBS for three times. Then the cells were stained with fluorescein isothiocyanate (FITC, Sigma-Aldrich) and 4', 6-diamidino-2-phenylindole (DAPI, Sigma-Aldrich) following the manufacturer's instructions. The cell morphology was detected by confocal laser scanning microscopy (CLSM; FluoView FV1000, Olympus, Tokyo, Japan) All measurements were tested in three replicates.

2.5. Bacteria culture

All three species were purchased from American Type Culture Collection (ATCC, Manassas, VA): *Streptococcus sanguinis* (*S. sanguinis,* ATCC10556), *Porphyromonas gingivalis* (*P. gingivalis,* ATCC33277) and *Fusobacterium nucleatum* (*F. nucleatum,* ATCC25586). The use of the bacterial species was approved by Institutional Review Board of Jilin University, School of Dentistry. All species were cultivated with tryptic soy broth (TSB, Sigma-Aldrich) supplemented with menadione (1 mg/L), L-cysteine hydrochloride (0.5 g/L, Sigma-Aldrich), yeast extract (5 g/L, Sigma-Aldrich) and hemin (5 mg/L, Sigma-Aldrich). *P. gingivalis* and *F. nucleatum* were cultured with anaerobic conditions of 80% N_2, 10% H_2 and 10% CO_2. *S. sanguinis* was cultured aerobically at 37 °C.

2.6. Time-killing assay of planktonic bacteria

Since the nanoparticles with a Ce6 concentration of above 5 μM had cell survival rates below 90%, Fe_3O_4-silane@Ce6/C6 and silane@Ce6/C6 MNPs at a Ce6 concentration of 2.5 μM were used in subsequent experiments. Therefore, the following five groups were tested for antibacterial effect:

(1) **Negative control group**: The bacteria were not treated by any photosensitizers or light sources (referred to as "control group");
(2) **silane@Ce6/C6 control group**: The bacteria were treated by silane@Ce6/C6 at a final concentration of 2.5 μM without light irradiation (referred to as "silane@Ce6/C6");
(3) **Fe_3O_4-silane@Ce6/C6 control group**: The bacteria were treated by Fe_3O_4-silane@Ce6/C6 at a final concentration of 2.5 μM without light irradiation (referred to as "Fe_3O_4-silane@Ce6/C6");
(4) **silane@Ce6/C6 aPDT group**: The bacteria were treated by silane@Ce6/C6 at a final concentration of 2.5 μM under 630 nm laser irradiation (referred to as "silane@Ce6/C6 + L");
(5) **Fe_3O_4-silane@Ce6/C6 aPDT group**: The bacteria were treated by Fe_3O_4-silane@Ce6/C6 at a final concentration of 2.5 μM under 630 nm laser irradiation (referred to as "Fe_3O_4-silane@Ce6/C6 + L").

The antibacterial activity of Fe_3O_4-silane@Ce6/C6 or silane@Ce6/C6 against suspended bacteria (*S. sanguinis, P. gingivalis* and *F. nucleatum*) were investigated by determining the time-kill curves. Briefly, *P. gingivalis*, *F. nucleatum* and *S. sanguinis* suspensions were diluted to 10^5 CFU mL^{-1}. The bacteria suspensions were treated with Fe_3O_4-silane@Ce6/C6 or silane@Ce6/C6 MNPs (2.5 μM Ce6), with or without irradiation with 630 nm light at an intensity of 100 $mW{\cdot}cm^{-2}$, for 3 min every hour (h). Upon 0, 0.5, 1, 2, 4, 8, 12 and 24 h incubation, the suspensions were 10-fold serially-diluted and spread onto Columbia blood agar. After incubation for 48 h at 37 °C, the CFU was counted. All measurements were performed in three replicates.

2.7. Effect of Ce6-based aPDT against biofilm formation on dentin squares

Extracted caries-free human molars were used to prepare dentin samples as the substrates for biofilm formation. The teeth collection was approved by Institutional Review Board of Jilin University, School of Dentistry (Ref. H20170062). After crown removal, square-shaped dentin samples with 5 × 5 mm and a thickness of about 1 mm were cut with a diamond saw. The dentin squares were grinded with 2400 grit SiC paper to standardize the samples. The dentin squares were sterilized by autoclaving (134 °C, 15 min) and stored in sealed sterilization pouches for subsequent use. Prior to each experiment, the dentin squares were treated by ultraviolet light for 30 min. To mimic the conditions in the oral cavity, the dentin squares were immersed in saliva at 37 °C for 2 h to pre-coat a salivary pellicle [23]. An equal volume of saliva from fifteen healthy donors was mixed to form the saliva sample. The donors had natural dentition without any oral bacterial diseases such as active caries, and had not taken any antibiotics in the last 3 months. Before donating saliva, the donors were requested not to brush teeth for 24 h and to refrain from food/drink intake for 2 h. Saliva was centrifuged at 3000 rpm for 20 min to remove cellular debris. The supernatant was filter-sterilized through sterile 0.22 μm filters (VWR International, Radnor, PA, USA). The sterile saliva was used to coat a salivary pellicle on dentin disks by immersing the disks in saliva for 2 h at 37 °C [23].

Each bacterial species was used to form single-strain biofilm following a previous study [23]. Each species was inoculated (10^8 CFU/mL) to the salivary pellicle-coated dentin squares in a 24-well plate and treated with Fe_3O_4-silane@Ce6/C6 or silane@Ce6/C6 MNPS at a Ce6 concentration of 2.5 μM. This was followed by irradiation with 630 nm light at an intensity of 100 mW·cm − 2 for 3 min. Groups without laser irradiation were set as control. The medium containing Fe_3O_4-silane@Ce6/C6 or silane@Ce6/C6 MNPs was refreshed every 24 h. After transferring to new 24-well plates, the dentin squares with adherent biofilms were treated with light irradiation in the same manner as the first day. Previous report indicated that relatively mature biofilms could be formed in about four days [24].

For live/dead bacteria analysis, each sample was stained by a mixture of SYTO 9 (2.5 μM) and propidium iodide (2.5 μM) following the instructions of the Live/dead bacterial kit (Molecular Probes, Eugene, OR, USA) [23]. Biofilms were imaged with confocal laser scanning microscopy. All experiments were repeated three times. Five images were randomly selected from each specimen of each group with three bacterial species, and 15 images for each group were obtained.

For CFU counts, a 5 × 3 full-factorial design was used with five material groups and three bacterial species. The biofilms were harvested from the specimens by mechanical scraping, then the bacterial deposits and the specimens were transferred into vials with 2 mL CPW, and were vibrated with sonication/vortex (Fisher, Pittsburg, PA, USA). A serial decimal dilution was performed with the suspensions of the biofilm. The suspensions were streaked onto Columbia blood agar and cultured at 37 °C for 48 h in an appropriate atmosphere with 5% CO_2 [23]. Then, the CFU was counted, along with the dilution factor.

MTT assay was used to investigate the metabolic activity of biofilms. A 5 × 3 full-factorial design was used with five material groups and three bacterial species. Briefly, the specimens with 4-day biofilms were rinsed three times with 200 μL of sterile phosphate buffered saline (PBS) to remove non-adherent bacteria. The specimens were then transferred to a new 24-well plate. The specimens were treated with MTT dye (1 mL) and incubated at 37 °C in 5% CO_2 for 1 h. Then the specimens were treated with equivalent dimethyl sulfoxide (DMSO, Sigma-Aldrich) to solubilize the formazan crystals in new 24-well plates. The plates were shaken horizontally for 20 min in the dark. The DMSO solution was pipetted into a 96-well plate. Then the absorbance at OD_{540nm} was measured using a microplate reader (SpectraMax M5, Molecular Devices, Sunnyvale, CA, USA) [23]. A higher absorbance indicates a higher metabolic activity in the biofilm on the specimens.

2.8. Fluorescence imaging and magnetic targeting of Fe_3O_4-silane@Ce6/C6 MNPs

To evaluate the in vitro fluorescence imaging, *S. sanguinis*, as bacterial species, was inoculated (10^8 CFU/mL) in 1.5 mL medium in a 24-well plate. Fe_3O_4-silane@Ce6/C6(2.5 μM Ce6)was added to each well for 24 h. Afterwards, the ratio emissions of Ce6/C6 was measured for 130 s with irradiation at 630 nm in the PDT process. The decreased ratio of Ce6/C6 represented the continuous consumption of Ce6 to monitor the clinical drug administration.

In order to evaluate the targeting antibacterial effect of Fe_3O_4-silane@Ce6/C6 on a developing biofilm, 2.7 mL of inoculation medium and 300 μL of *S. sanguinis* were inoculated at a final concentration of 10^8 CFU/mL in petri dishes and cultured aerobically at 37 °C for 48 h in the presence of Fe_3O_4-silane@Ce6/C6 (2.5 μM Ce6), with or without a magnet being placed at the bottom center of the dish [25]. The petri dishes were exposed to the 630 nm light at 100 mW·cm^2 for 5 min every 24 h. Subsequently, the dishes were washed with PBS and the unbound bacteria were removed. The bacteria viability at the margin area of the magnet was assessed using the live/dead assay as described above. The experiments were performed in triplicate with separately cultured bacteria.

2.9. Statistic analysis

All data were checked for normal distribution with the Kolmogorov-Smirnov test. Two-way ANOVA was used to assess the differences in biofilm properties and nanoparticles for CFU counting and MTT assay. Tukey's post-hoc test was used to compare the data ($p < 0.05$). Statistical analyses were performed by SPSS 19.0 (SPSS, Chicago, IL).

3. Results

3.1. Preparation and characterization of multifunctional nanoparticles

Nanoparticles of Fe_3O_4-silane@Ce6/C6 were synthesized as shown in Fig. 1. Ce6 and C6 were co-coated by the hydrophobic interspace between octadecyl groups of oleic acid on the surface of Fe_3O_4 NPs and the alkyl chains of silane, forming the multifunctional platform via hydrophobic interaction.

The TEM image of Fe_3O_4 NPs in Fig. 2A with spherical phases indicates approximately 8 nm in diameter. Fig. 2B shows that the diameter of Fe_3O_4-silane@Ce6/C6 MNPs was approximately 100 nm with magnetically-driven aggregation. Furthermore, as shown in Fig. 2C, HR-TEM image displays clear lattice fringes with 0.253 nm lattice in (311) planes. Fig. 2D depicts the average size of Fe_3O_4-silane@Ce6/C6 MNPs (122.4 nm). The size distribution was relatively narrow and all MNPs had sizes below 150 nm. Magnetization hysteresis loops of Fe_3O_4 nanoparticles (Fig. 2E) demonstrated good superparamagnetism. The diffraction diagram in Fig. 2F shows characteristic peaks close to the literature values for standard Fe_3O_4 powder diffraction data, which matched the magnetite (Fe_3O_4) crystal structure data (JCPDS card no. 19-0629). The synthetic Fe_3O_4 NPs were crystals with an inverse spinel structure. Fig. 2H shows the emission spectra of silane@Ce6/C6, C6 and Ce6, respectively. The maximum emission spectrum of C6, marked red, was at 510 nm, and the emission peak of Ce6, marked blue, was at 650 nm, which could be co-excited by 405 nm wavelength light. Fig. 2G shows the emission spectra of Fe_3O_4-silane@Ce6/C6, C6, and Ce6, respectively. The IONPs did not affect the emission peaks of C6 and Ce6.

The surface Zeta potential of silane@Ce6/C6 (Fig. 3A) and Fe_3O_4-silane@Ce6/C6 MNPs (Fig. 3B) are approximately -28° , indicating good stability. In contrast to the transparent color and precipitation of Ce6, the color of Fe_3O_4-silane@Ce6/C6 and silane@Ce6/C6 MNPs changed to a dark green, and no precipitation was found at the bottom of Eppendorf tubes (Fig. 3C-F), implying the existence of Ce6 in varieties of solutions (pH from 4.5 to 8.0).

3.2. Singlet oxygen $^1O_2$ detection and cytotoxicity assessment

As shown in Fig. 4A, the absorption spectra of Fe_3O_4-silane@Ce6/C6 was detected at interval 1 min with red light irradiation (630 nm). The absorbance of ABDA decreased at 260 nm along with the irradiation time, due to the reaction of ABDA and the generation of $^1O_2$ from Fe_3O_4-silane@Ce6/C6 MNPs. In addition, the band at 402 nm showed similar tendency due to the consumption of Ce6 molecules via the photodegradation of red light. This indicates the presence of Ce6 in Fe_3O_4-silane@Ce6/C6 MNPs.

3.3. In vitro cytotoxicity assay

CCK-8 assay was performed to investigate the dark cytotoxicity of Fe_3O_4-silane@Ce6/C6 and silane@Ce6/C6 MNPs with L929 mouse fibroblast cells (Fig. 4B). The cells were more than 90% viable with the concentration of 2.5 μM or less. As the concentration was increased to 10 μM, the cell viability slightly decreased, but was still more than 80%. As illustrated in Fig. 4C, the L929 cells were incubated with Ce6 concentrations of 0, 2.5 and 5 μM, followed by DAPI and FITC staining. The DAPI-labeled nuclei were blue fluorescence, homogeneous and intact, indicating no apoptosis. When the cells were incubated with Ce6 concentration of 10 μM, only a few condensed and lightened nuclei could be found in round and shrunken cells, indicating very few necrotic cells.

3.4. Antibacterial efficacy of Fe_3O_4-silane@Ce6/C6 MNPs against periodontitis-related pathogens

The time-killing kinetics of nanoparticles is plotted in Fig. 5. Fe_3O_4-silane@Ce6/C6 and silane@Ce6/C6 MNPs without light irradiation showed a similar trend of killing kinetics to the control group, indicating no antibacterial effects by the nanoparticles alone. For all three species, the trend of the killing kinetics in silane@Ce6/C6 + L group was similar to Fe_3O_4-silane@Ce6/C6 + L. In addition, this killing behavior was time-dependent. There were differences among the different bacterial species. In the presence of Fe_3O_4-silane@Ce6/C6 and silane@Ce6/C6 MNPs under light irradiation, *S. sanguinis* had a shorter killing time of 2 h, while the other two species took 4 h to kill.

Representative results of live/dead analysis were shown in Fig. 6. The control group and that without light irradiation had primarily green staining with live bacteria. In sharp contrast, Fe_3O_4-silane@Ce6/C6 and silane@Ce6/C6 MNPs with light irradiation had mainly dead bacteria with stained red.

The CFU results for single-strain biofilms on dentin are shown in Fig. 7(A—C). The CFU values for the differences nanoparticles without light irradiation were similar to the control group ($p > 0.1$). Fe_3O_4-silane@Ce6/C6 and silane@Ce6/C6 MNPs with light irradiation had similar CFU, indicating that IONP incorporation into the nanoparticles did not compromise the aPDT effect on periodontitis biofilms. Compared to the control groups and nanoparticles without light irradiation, the CFU of nanoparticles with aPDT had significant reductions for all three species ($p < 0.05$). Nanoparticles with light irradiation decreased the CFU of different bacterial species differently. *F. nucleatum* was decreased by slightly less than 4 log, while *P. gingivalis* was reduced by more than 5 log ($p < 0.05$). There was no significant interaction between the two factors (bacterial species and different materials) ($p > 0.1$).

The metabolic activity of the 4-day single-species biofilms is shown in Fig. 7 for: (D) *S. sanguinis,* (E) *P. gingivalis,* and (F) *F. nucleatum* (mean ± sd; $n = 6$). A similar trend to the CFU results was detected the metabolic activity. For each species, Fe_3O_4-silane@Ce6/C6 MNPs without light irradiation had similar metabolic activity with the control group ($p > 0.1$). Fe_3O_4-silane@Ce6/C6 MNPs with light irradiation exhibited significantly lower metabolic activity than nanoparticles without irradiation ($p < 0.05$). These data demonstrate that nanoparticle-mediated aPDT differently decreased the metabolic activity for

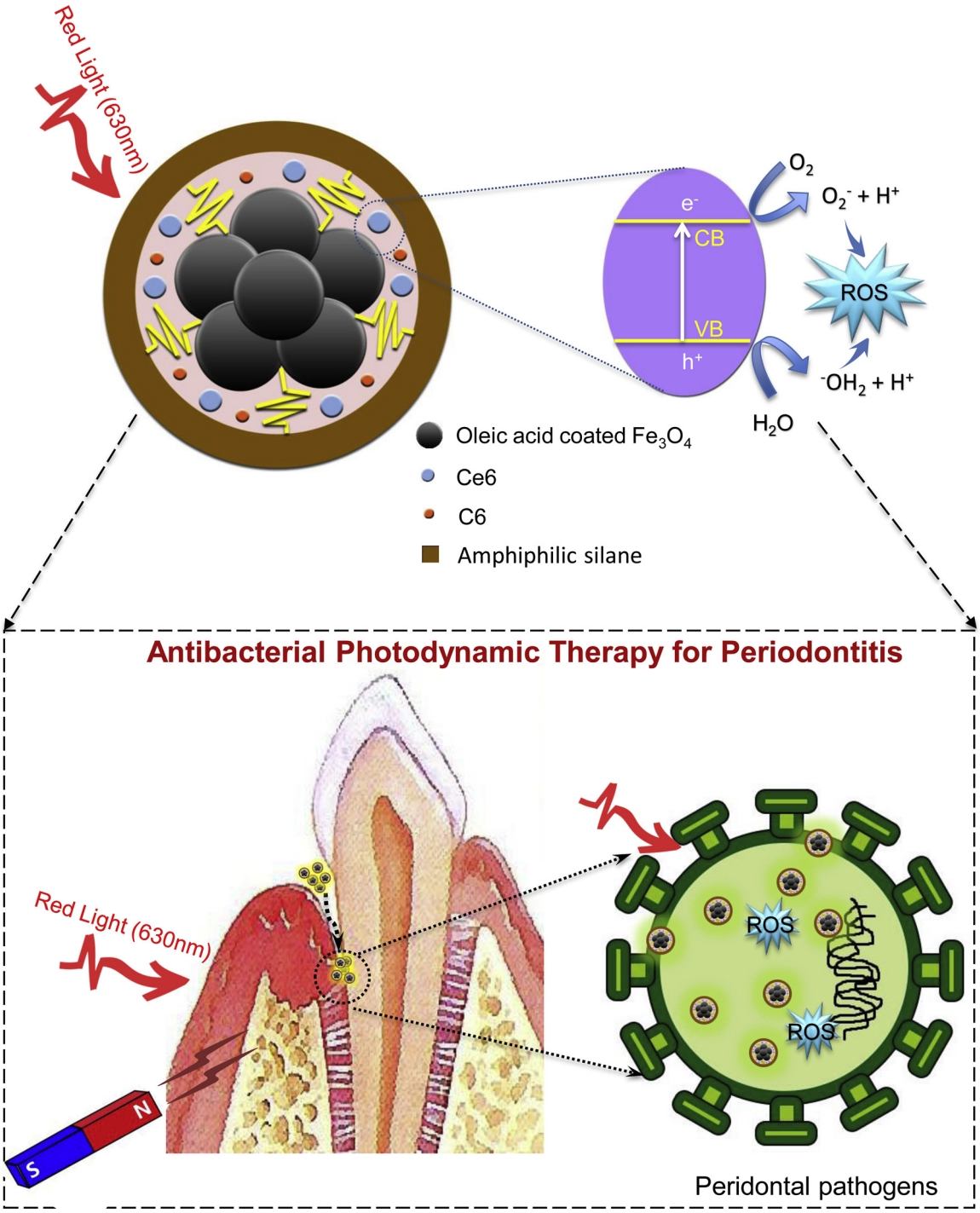

Fig. 1. Schematic illustration of Fe_3O_4-silane@Ce6/C6 MNP-mediated antimicrobial photodynamic therapy with a magnetic field. The nanoparticles could be attracted to the site of infection against the drainage of gingival crevicular fluid and high saliva fluid turnover. The reactive oxygen species generated by a combination of photoexcited nanoparticles and light irradiation play a critical role in killing periodontal pathogens. Note: Chlorin e6 (Ce6) and Coumarin 6 (C6) dye were co-coated by the hydrophobic interspace between octadecyl groups of oleic acid on the surface of Fe_3O_4 MNPs and the alkyl chains of silane, forming the multifunctional platform via hydrophobic interaction.

all three periodontitis-related species.

3.5. Fluorescence imaging and magnetic targeting in vitro

When the irradiation time was increased to 130 s, the ratio of the gray value strength of the Ce6 and C6 images decreased (Fig. 8A). The first two insets were the laser confocal images before light irradiation. The last two insets were the laser confocal images after 130 s light irradiation. This illustrates the consumption of Ce6 (Fig. 8A). This demonstrates that the Fe_3O_4-silane@Ce6/C6 MNPs could potentially be used for monitoring of the Ce6-mediated aPDT effect in the real time, which would be clinically beneficial in guiding drug administration and medication safety.

Compared to the group without an external magnetic field as shown in Fig. 8Bi, Fe_3O_4-silane@Ce6/C6 MNPs could be magnetically directed to become concentrated in a particular part of a biofilm. The

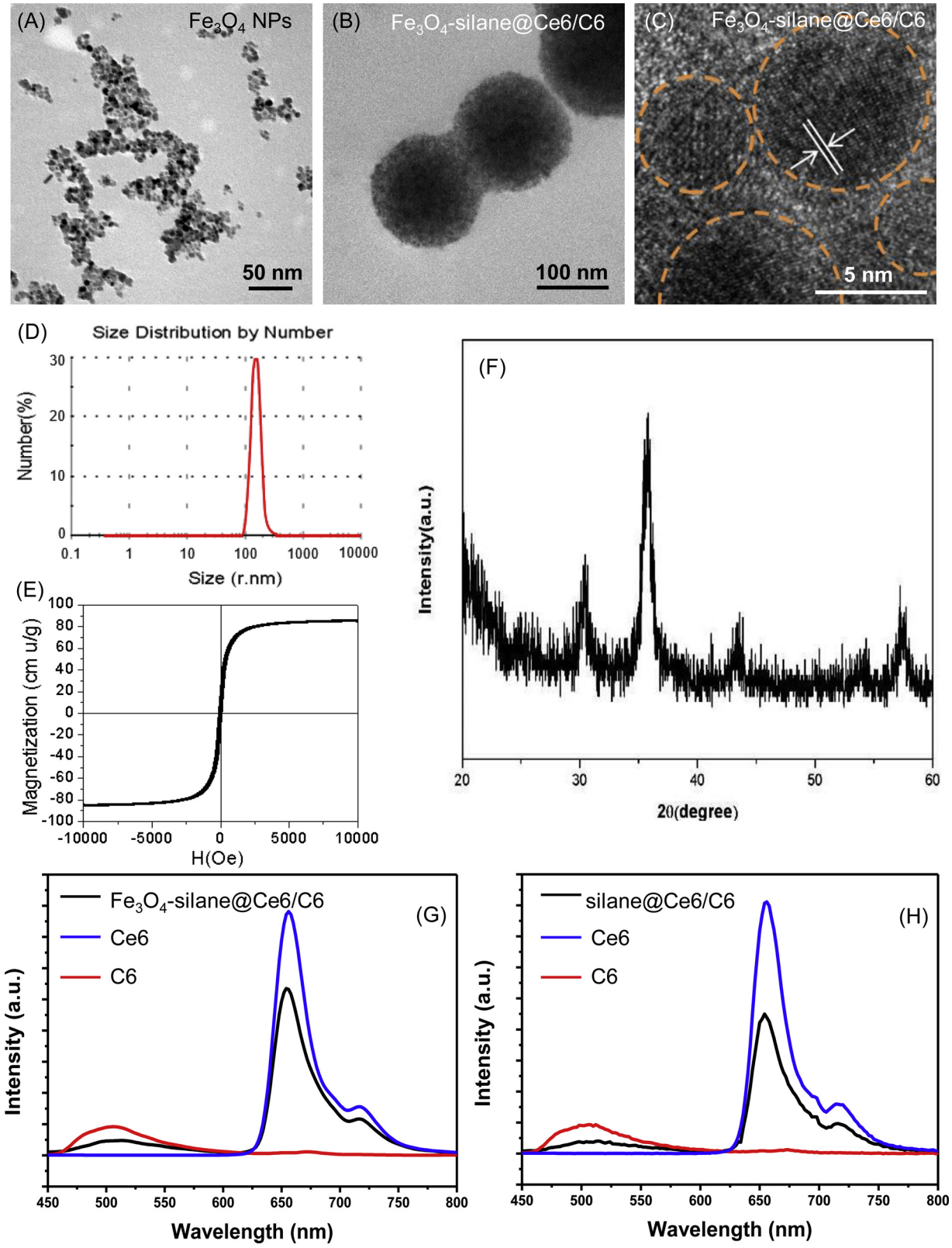

Fig. 2. Characterization of multifunctional nanoparticles. (A) TEM image of hydrophilic OA-Fe_3O_4 nanoparticles; (B) TEM of Fe_3O_4-silane@Ce6/C6 MNPs; (C) HR-TEM of Fe_3O_4-silane@Ce6/C6 MNPs, showing clear (311) lattice fringes with 0.253 nm interplanar spacing; (D) Dynamic light scattering (DLS) size distributions of Fe_3O_4-silane@Ce6/C6 MNPs (122.4 nm); (E) Magnetization hysteresis loops of Fe_3O_4-silane@Ce6/C6 MNPs; (F) XRD pattern of Fe_3O_4-silane@Ce6/C6 MNPs; (G) Fluorescence emission spectra of Fe_3O_4-silane@Ce6/C6 MNPs, Ce6, and C6 with 405 nm excitation. (H) Fluorescence emission spectra of silane@Ce6/C6 MNPs, Ce6, and C6 with 405 nm excitation.

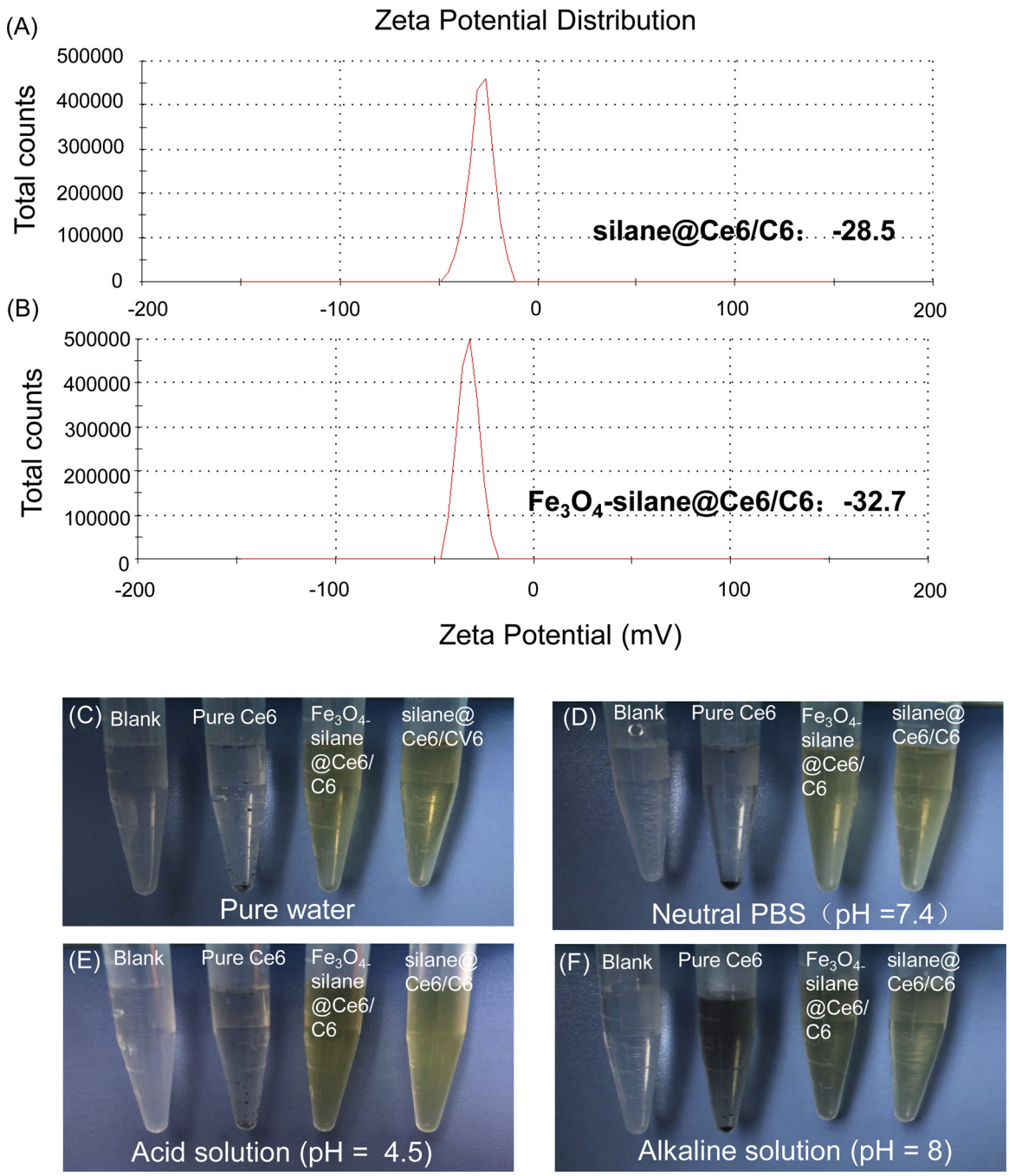

Fig. 3. The zeta potential of (A) silane@Ce6/C6 MNPs and (B) Fe_3O_4-silane@Ce6/C6 MNPs: The zeta potential of silane@Ce6/C6 MNPs are -28.5 and Fe_3O_4-silane@Ce6/C6 MNPs are -32.7, which indicates a highly solubility in water and the stability of the prepared MNPs. (C–F) Images of dispersions of pure Ce6, Fe_3O_4-silane@Ce6/C6 MNPs and silane@Ce6/C6 MNPs in (C) pure water, (D) neutral PBS, (E) acid solution and (F) alkaline solution. The two types of nanoparticles were well-dispersed without visible aggregation. In contrast to the transparent color of pure Ce6, the color of Fe_3O_4-silane@Ce6/C6 MNPs and silane@Ce6/C6 MNPs changed to a dark green, implying the existence of Ce6 in all solutions (For interpretation of the references to colour in this figure legend, the reader is referred to the web version of this article).

fluorescence images of 2 day-biofilm of *S. sanguinis* had a strong increase in dead bacteria in the region where Fe_3O_4-silane@Ce6/C6 MNPs were magnetically concentrated. In contrast, mainly live bacteria were detected in the area outside the magnetic concentration of Fe_3O_4-silane@Ce6/C6 MNPs (Fig. 8Bii).

4. Discussion

This study developed multifunctional Fe_3O_4-silane@Ce6/C6 nanoparticles having a Ce6-mediated aPDT effect, and investigated the inhibitory effects against periodontitis-related pathogens for the first time. All the hypotheses were proven. The multifunctional nanoparticles exhibited good water-solubility, chemical stability, and biocompatibility without cytotoxicity. The photoexcited Fe_3O_4-silane@Ce6/C6 MNPs had potent antibacterial functions against all three species of periodontitis-related pathogens, yielding substantially lower metabolic activities and biofilm CFU. In addition, the aPDT effect of Ce6 could be real-time monitored by the ratio metric of fluorescence of Ce6/C6. Fe_3O_4 NPs incorporation in the nanoparticles did not negatively impact the aPDT efficiency, while providing the beneficial

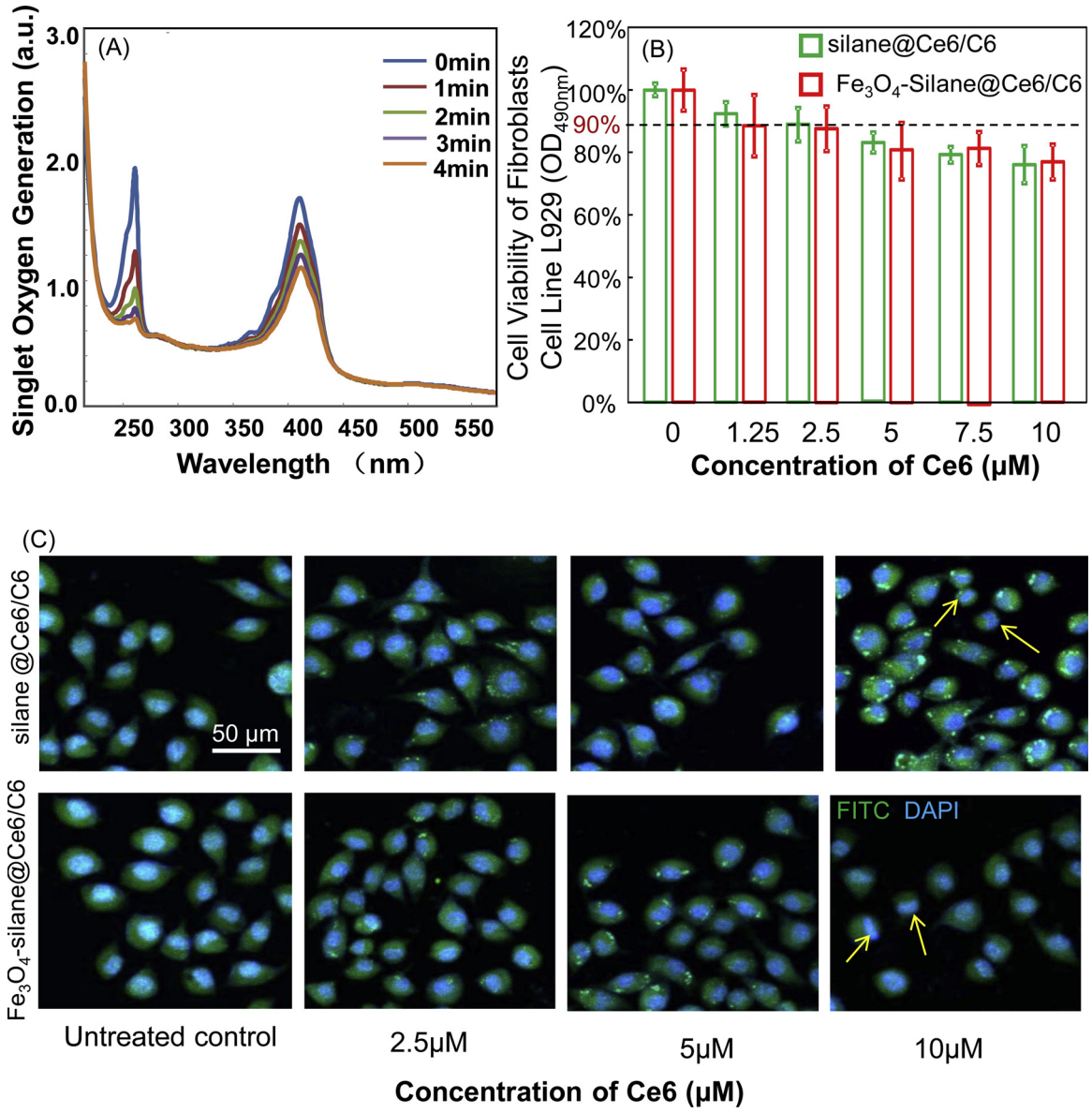

Fig. 4. Generation of singlet oxygen generation and dark cytotoxicity of nanoparticles. (A) UV–vis absorption changes of singlet oxygen indicator ABDA mixed with Fe_3O_4-silane@Ce6/C6 MNPs (13.6 μg/mL) for successive time duration of red-light irradiation (630 nm, 100 mW/cm^2). (B, C) Dark cytotoxicity of Fe_3O_4-silane@Ce6/C6 MNPs and silane@Ce6/C6 MNPs on mouse fibroblast cell line L929: (B) Viability of L929 cells vs. Ce6 concentration of Fe_3O_4-silane@Ce6/C6 MNPs or silane@Ce6/C6 MNPs after 24 h without irradiation in the dark (mean ± sd). Dotted line represents the safety border of 90% cell viability. (C) CLSM images of L929 cells incubated with Fe_3O_4-silane@Ce6/C6 MNPs or silane@Ce6/C6 MNPs containing 0, 2.5, 5, and 10 μM of Ce6. Arrows: apoptotic cells. Bar: 50 μm.

magnetic targeting capability.

The multifunctional nanoparticles possessed properties of regular morphology, well size-distribution and high hydrophilicity, which would be beneficial for application in the biomedical field with a good biocompatibility. Recent studies have shown that using superparamagnetic IONPs with a magnetic field could target infection sites, inhibit bacterial functions and penetrate biofilms; thereby conquering the therapeutic obstacles always came across with traditional antibacterial agents alone [26]. In the present study, ultra-small Fe_3O_4 NPs were synthesized and loaded into the silane coating of nanoparticles via hydrophobic interactions. Based on this design, the nanoparticles could be easily attracted to the site of infection against the drainage of gingival crevicular fluid and high saliva fluid turnover. From the luminescent spectra of Ce6, it not only had the aPDT function, and also potentially could serve as an imaging agent. In fact, the intensity of C6 emission spectrum remained constant when the aPDT consumed the Ce6 molecules. Therefore, C6 molecules could serve as real-time monitoring probe during the aPDT. The normal pH of saliva in the mouth is in the range of 6.3–7.0. However, the pH of saliva could decrease to 3.5 temporarily due to acidic beverage ingestion, or increase to 8.3 during alkaline food intake [27]. Therefore, the excellent dispersity and solubility of the nanoparticles would facilitate a high drug delivery efficacy when being applied in oral applications. Regarding the application in periodontitis, most photosensitizers alone would lose activity in the presence of saliva, or with a marked flow of gingival crevicular fluids. In addition, subgingival biofilms are highly packed and characterized by complexity and pathogenicity. The application of nanoparticles to aPDT would help overcome some of the problems related to serum constituents and increase the ability of penetration into biofilms. This could then improve the pharmacological characteristics of the photosensitizer [16].

Reactive oxygen species generated by the combination of photoexcited nanoparticles and light irradiation plays a critical role in killing periodontal pathogens. The characterization of Ce6, as the source of

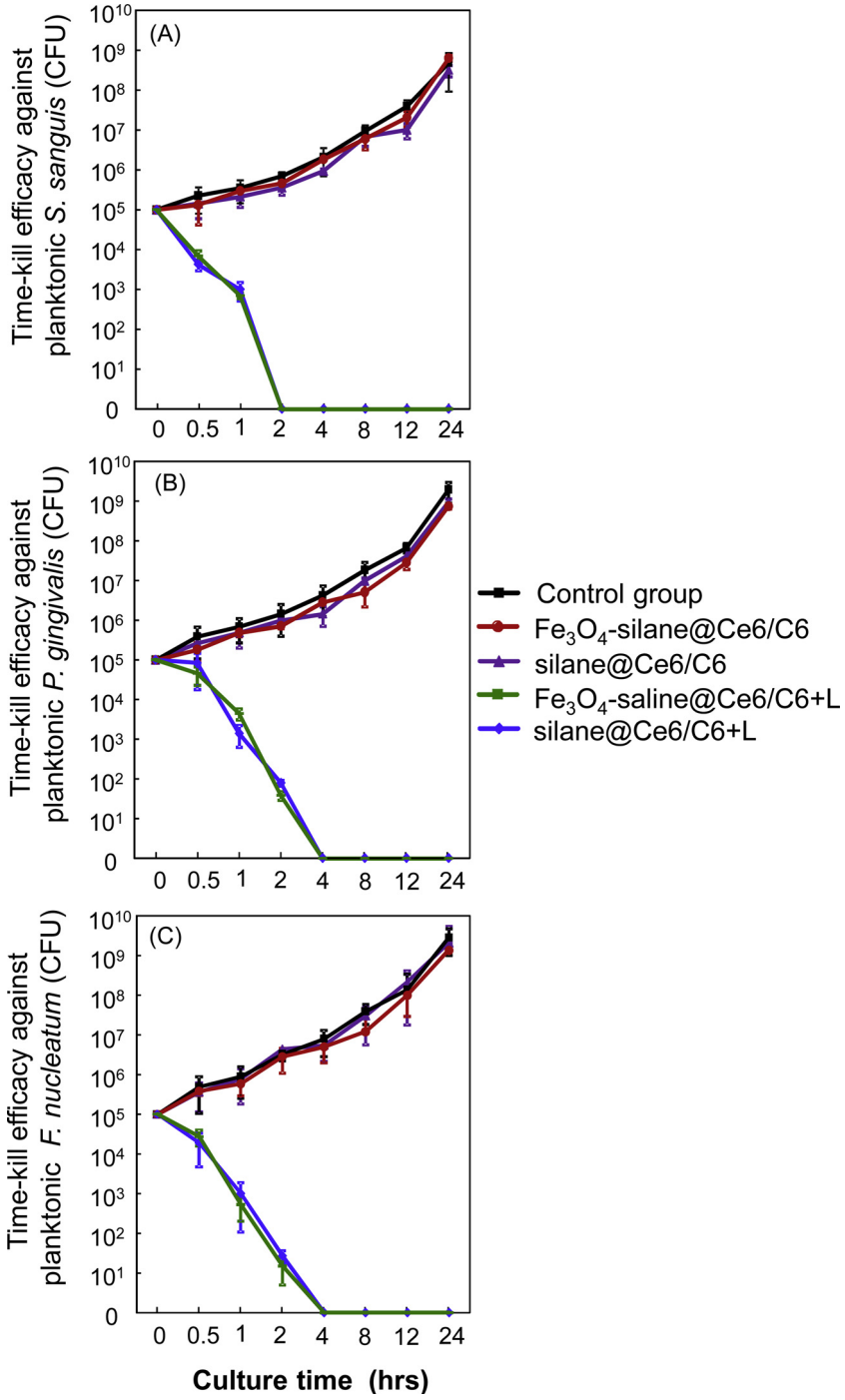

Fig. 5. Time-kill curve of Fe_3O_4-silane@Ce6/C6 MNPs and silane@Ce6/C6 MNPs in the presence and absence of red-light irradiation (630 nm, 100 mW/cm^2, 3 min) against (A) *S. sanguinis*, (B) *P. gingivalis* and (C) *F. nucleatum*. Note the log scale for the y axis for colony-forming units (CFU). The surviving bacteria were plated at various time points as shown on the x axis. All data points represent mean ± sd of three independent experiments.

singlet oxygen ($^1O_2$) with the 630 nm red light, was tested by the photobleaching of ABDA molecules [28]. The present study confirmed the generation of $^1O_2$ from Fe_3O_4-silane@Ce6/C6 MNPs photoexcited by red light irradiation. Red light at a wavelength of 630 nm was applied as an exciting light source mainly due to its excellent penetration through human tissues. Inflammatory periodontium was characterized as bone resorption and soft tissue swelling. Therefore, red light (630 nm) could easily penetrate through the periodontium and reach the deep site of the periodontal pocket. Fiber-optic laser light should be avoided for use subgingivally, because it may lead to bleeding and damage in the periodontal tissues. In addition, the $^1O_2$ was produced by photosensitizers via the type II reaction, in which the excited photosensitizer reacted with $^3O_2$ to produce energy transfer [29]. The $^1O_2$ was highly reactive and most desirable in aPDT, since it could induce the damage of biomolecules and the oxidation of cellular structures, leading the inactivation of the membrane transport system, inhibition of plasma membrane enzyme activities, and lipid peroxidation [30]. Previous studies demonstrated that aPDT via different PS could eliminate periodontal pathogens or artificial biofilms, with a maximum reduction of 99.9% [9,31]. Hence, $^1O_2$ could penetrate into dental plaque and subsequently kill the bacteria. Regardless of the penetration of PS into the biofilms, $^1O_2$ exterior to the cell is as effective as that in

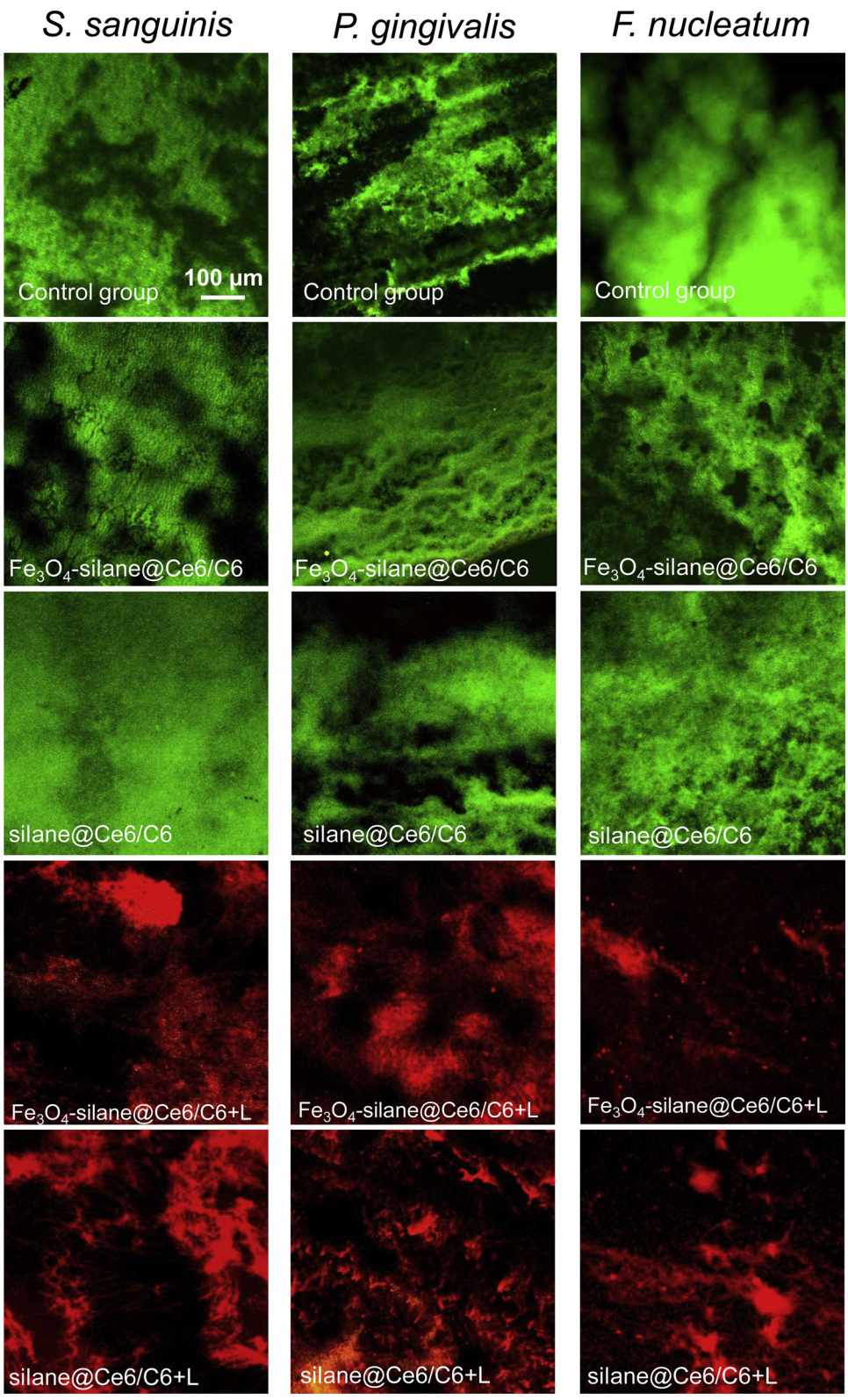

Fig. 6. Representative live/dead images of 4-day biofilms of three of *S. sanguinis* (left column), *P. gingivalis* (middle column) and *F. nucleatum* (right column) on dentin for (A–C) Untreated control, (D–F) Fe_3O_4-silane@Ce6/C6 MNPs without red light, (G–I) silane@Ce6/C6 MNPs -treated bacteria without red light, (J–L) Fe_3O_4-silane@Ce6/C6 MNPs in the presence of red light irradiation (630 nm, 100mW/cm^2, 3min), and (M–O) silane@Ce6/C6 MNPs in presence of red light irradiation (630 nm, 100mW/cm^2, 3min). All images had the same scale bar as shown in (A). Live bacteria were stained green. Dead bacteria were stained red. The control, Fe_3O_4-silane@Ce6/C6 MNPs and silane@Ce6/C6 MNPs in the absence of red light had primarily live bacteria. While, Fe_3O_4-silane@Ce6/C6 MNPs and silane@Ce6/C6 MNPs with red-light irradiation showed mainly red staining of compromised bacteria (For interpretation of the references to colour in this figure legend, the reader is referred to the web version of this article).

the inside; hence, $^1O_2$ at the cell's exterior is sufficient to suppress the biofilms [32]. Therefore, in the present study, $^1O_2$ produced by Fe_3O_4-silane@Ce6/C6 MNPs with 630 nm laser irradiation likely played an important role in the antimicrobial effect against periodontitis-related pathogens.

Good biocompatibility is an important prerequisite for the application of nanoparticles in the biomedical field. Nanoparticles with cationic macromolecules could lead to side effects because of interactions with cell membranes or extracellular matrix proteins [33]. Previous study indicated that nanoparticles containing Ce6 were biosafe to murine breast carcinoma 4T1 cells at a concentration below 15 μM [34]. Taking into account the higher proliferation and chemo-resistance of cancer cells, nanoparticles at a concentration range from 0 to 10 μM were determined to be appropriate in evaluating biocompatibility

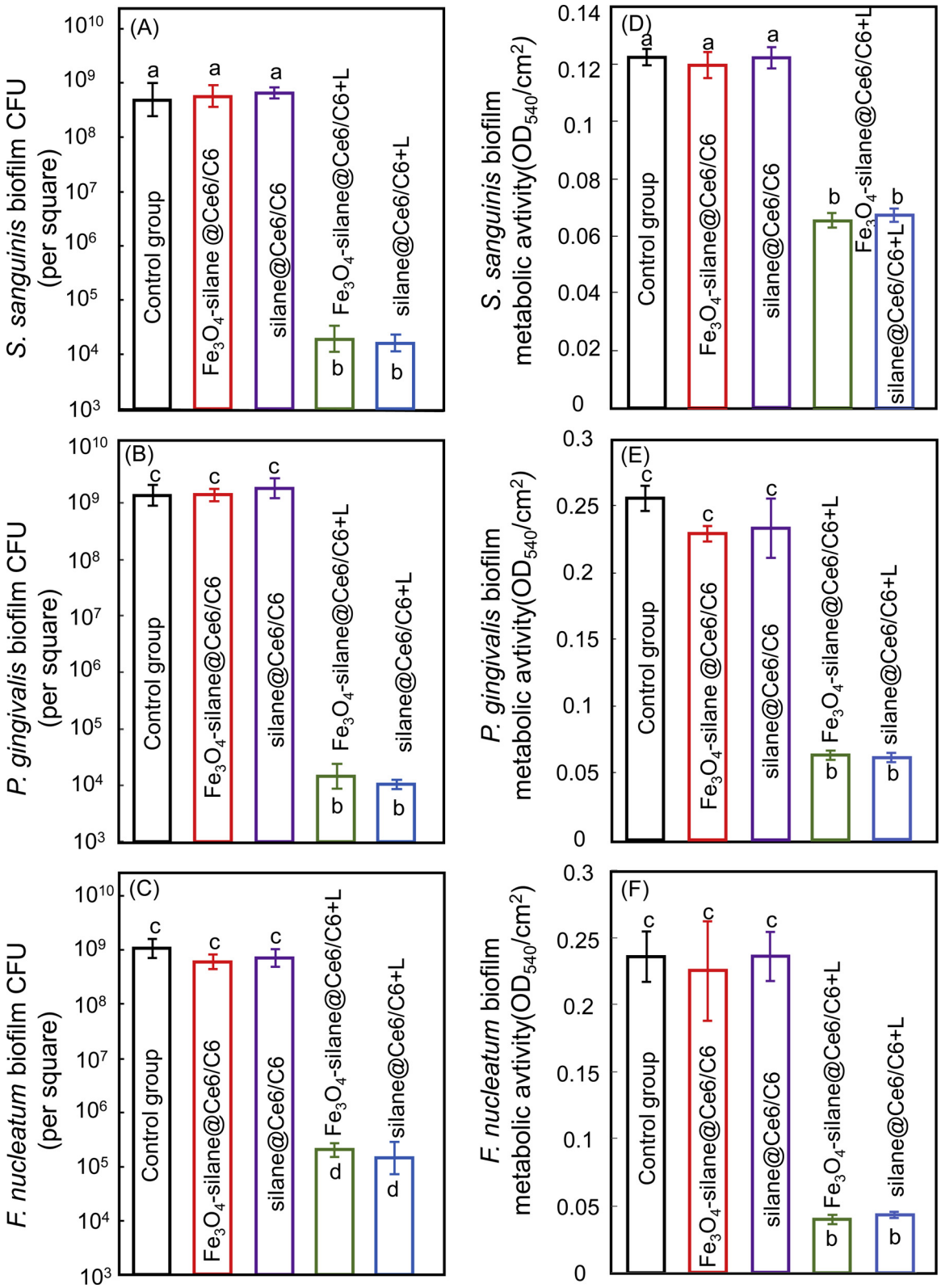

Fig. 7. CFU of 4-day biofilms of (A) *S. sanguinis*, (B) *P. gingivalis* and (C) *F. nucleatum* after aPDT application (mean ± sd; $n = 6$). Note the log scale for the y-axis. MTT assay for the metabolic activity of 4-day biofilms of (D) *S. sanguinis*, (E) *P. gingivalis* and (F) *F. nucleatum* after aPDT (mean ± sd; $n = 6$). In (A–C) or (D–F), dissimilar letters indicate values that are significantly different from each other ($p < 0.05$).

against normal cells (L929 fibroblasts). The results showed that the cells were more than 90% viable with the concentration of 2.5 μM or less. This low cytotoxicity of the nanoparticles in this study was likely attributable to the negatively-charged surface which could reduce cytotoxicity. Therefore, the Fe_3O_4-silane@Ce6/C6 and silane@Ce6/C6 MNPs showed little dark toxicity and had great potential to be new photosensitizers in dental application.

In the present study, *S. sanguinis*, *P. gingivalis* and *F. nucleatum* were

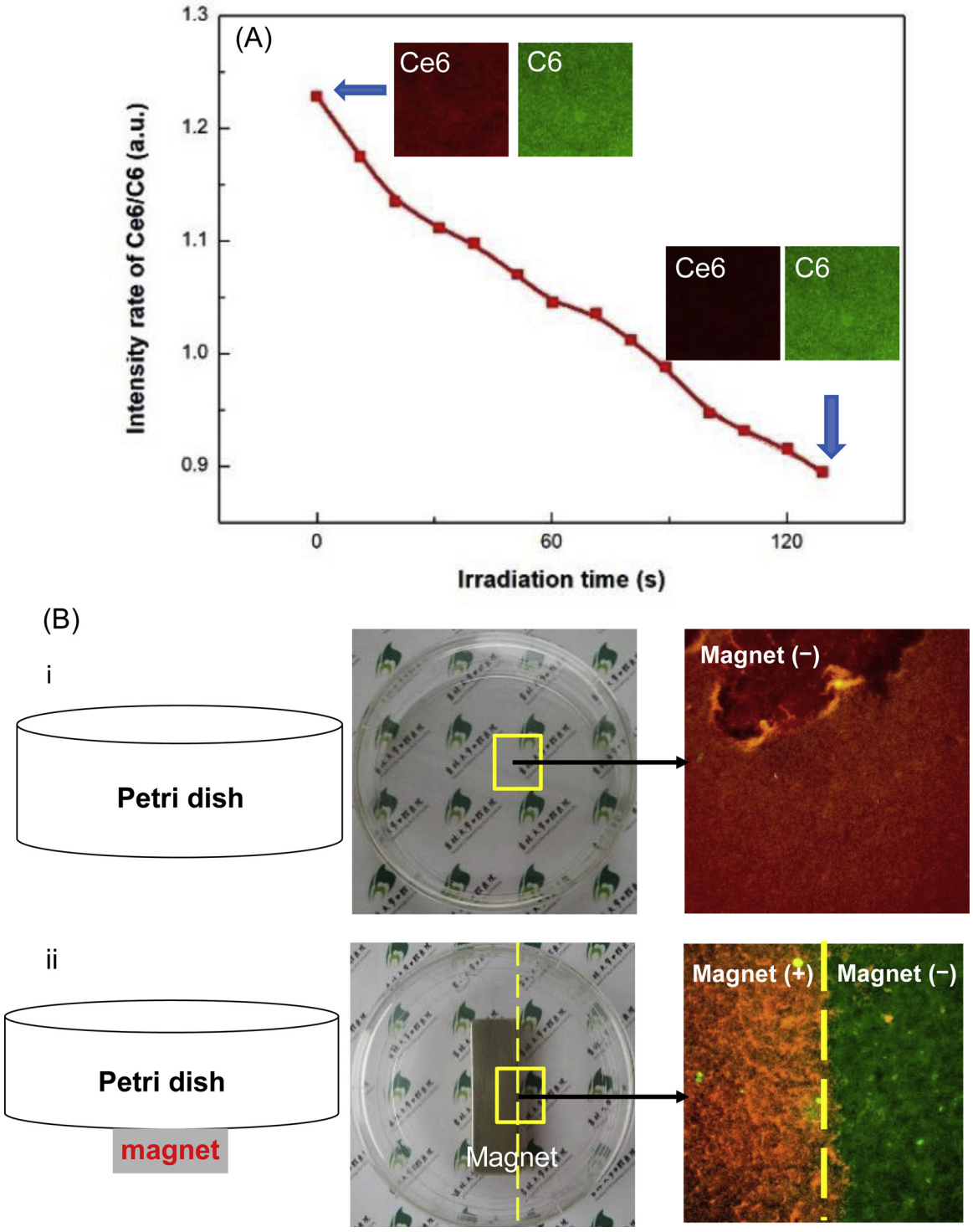

Fig. 8. Real-time monitoring and magnetic targeting functions of multifunctional nanoparticles: (A) Ratio metric intensity of Ce6/C6 based on the grayscale value of the confocal images from different detection channels in the irradiation time 0–130 s. Inset: the first two and last two images for illustration of the Ce6 consumption. (B) Comparison of aPDT effect in the presence of Fe_3O_4-silane@Ce6/C6 MNPs (2.5 μM Ce6) with and without external magnetic field: (i) aPDT effect of Fe_3O_4-silane@Ce6/C6 MNPs without magnetic targeting. Left panel: schematic diagram, middle panel: photograph showed culture dish without the magnet, right panel: live/dead image in yellow pane. (ii) aPDT effect of Fe_3O_4-silane@Ce6/C6 MNPs with magnetic targeting. Left panel: schematic diagram, middle panel: photograph showed culture dish with the magnet, right panel: live/dead image in the yellow pane. Live bacteria were stained green. Dead bacteria were stained red. Samples without magnet showed primarily dead bacteria. Samples with magnet had primarily dead bacteria in the magnetic region (For interpretation of the references to colour in this figure legend, the reader is referred to the web version of this article).

selected as representatives of bacteria that colonized in dental plaque biofilms at the early, middle and late stages of biofilm development. First, *S. sanguinis* plays a pioneering role as well as an assisting role in biofilm formation. *S. sanguinis* can recognize receptors in the salivary pellicle, and it is the predominant species that initially colonizes the dental surfaces [35]. In addition, the extensive intrageneric co-aggregation and production of extracellular polysaccharides by *streptococci* play an important role in the early stage of biofilm formation [36].

Moreover, although previous studies indicated that *S. sanguinis* was a benign or even a beneficial microorganism of the oral cavity, its association with bacterial endocarditis was established recently [37]. Therefore, the presence of *S. sanguinis* could be potentially dangerous, particularly when it could reach the bloodstream during periodontal interventions [38]. Second, *P. gingivalis* is frequently found in disease sites, suggesting that *P. gingivalis* plays an important role in the pathogenicity of periodontal diseases. Third, *F. nucleatum* is not only detected in advanced periodontitis, but also plays potential synergistic effects with *P. gingivalis* on the bacterial virulence [39]. Therefore, these three species were selected to form single-strain periodontitis-related biofilms to investigate the antibacterial PDT effects of Fe_3O_4-silane@Ce6/C6 and silane@Ce6/C6 MNPs.

Currently, dynamic flow systems are applied in biofilm formation experiments since it can simulate the physiological flow conditions in the oral cavity [40,41]. In addition, static biofilm models are also frequently used [16,23]. The present study used a static biofilm model for the following reasons. (1) This model was economical and practical, because specialized equipment was not required, and it could simultaneously perform a large number of tests. (2) This model could be more easily performed than dynamic flow systems. (3) In the present study, since the biofilms were treated with light irradiation every day, the biofilms formation via the static system facilitated the aPDT intervention investigation. (4) Previous studies also used static models to evaluate anti-biofilm effects of various polymers, composite materials, and nanoparticles [23,42,43]. (5) Previous study compared the static method with the dynamic method for biofilm formation, and confirmed that both were useful for mimicking the periodontitis-related biofilms [44]. Moreover, to mimic the conditions in the oral cavity, the dentin squares were immersed in saliva at 37 ℃ for 2 h to pre-coat a salivary pellicle. Numerous studies verified that the 2-h immersion in saliva at 37 ˚C was adequate for forming salivary pellicles on surfaces [23,45]. Li et al. investigated the effects of salivary pellicles on bonding agent resins containing antibacterial agents against biofilms [45]. The precoating of salivary pellicles on the resin surface significantly decreased its antibacterial efficacy, compared to resin without salivary pellicles. These results indicate that this procedure was able to establish a well-formed saliva pellicle on the dentin surface via a 2-h immersion in saliva at 37 ˚C. Similarly, Gong et al. successfully developed salivary pellicles on acrylic resin disks by a 1-h immersion in saliva at 37 ˚C [46].

The inhibitory effect of aPDT on bacterial growth, mediated by nanoparticles, occurred early and could maintain for a relatively longer time. In the present study, *S. sanguinis* was the easiest to kill, compared to the other two bacterial species. This may be associated with the special wall component of *S. sanguinis* which may be sensitive to the singlet oxygen produced by aPDT, likely via the membrane-associated adenosine triphosphate ATPases [47]. Additionally, as mentioned above, *S. sanguinis* was a pioneering colonizer in the formation of dental plaque and acted as a scaffold. Therefore, it is highly beneficial that *S. sanguinis* was the most easily killed by aPDT in the present study.

Biofilms are much more difficult to kill than planktonic bacteria, because the extracellular polymeric substance inside the biofilm resists the entry of conventional antibacterial agents. Subgingival biofilms are the main factor causing periodontitis. In the present study, the nanoparticles with light irradiation greatly downregulated the metabolic activity of biofilms, compared to the controls. This was likely due to the generated $_1O^2$ through the oxidation of amino acids and DNA damage [48]. Biofilms exhibit a reduced susceptibility to traditional aPDT due to the reduced penetration of the photosensitizers into the biofilm matrix [14]. In the present study, the significant bactericidal activity against planktonic periodontitis-related pathogens and biofilms showed the efficacy of Fe_3O_4-silane@Ce6/C6 MNPs as a photosensitizer for aPDT. Interestingly, planktonic or biofilms of the three species treated solely with either Fe_3O_4-silane@Ce6/C6 or silane@Ce6/C6 MNPs without light irradiation remained viable. Similarly, the treatment of irradiation in the absence of the photosensitizer did not produce the bacterial photoinactivation in previous studies [49]. The CFU assay is the most essential for evaluating a new antimicrobial approach, as the American Society of Microbiology (ASM) stated in 2010. Previous studies demonstrated that aPDT via Ce6 yielded approximately 2–4 log of CFU reduction [10,50]. However, CFU quantification showed that with Fe_3O_4-silane @C6/Ce6 MNPs as a photosensitizer, the bacterial CFU counts of 4-day biofilms showed a logarithmic reduction of 4–5 log in the present study. This high efficacy against periodontitis-related biofilms was likely due to the high hydrophilic surface of the nanoparticles. Moreover, nanoparticles can more easily disrupt the biofilm matrix, allowing for a deeper penetration as well as an increased drug stability and retention [16]. Additionally, oxidative stress is reported to be a key mechanism for the antibacterial activity of nanoparticles via reactive oxygen species generation [51]. Several studies also displayed that *F. nucleatum*exhibited various sensitivity to different antibacterial agents [23,52,53]. For example, *F. nucleatum* was easier to kill than *P. gingivalis* by nano-silver and nano-copper [52]. However, *F. nucleatum* was less sensitive to nano-zinc or quaternary ammonium methacrylates than *P. gingivalis* [23,51]. Furthermore, for dual-species biofilms, the CFU counts of *F. nucleatum*had less reduction than *P. gingivalis*by a povidone–iodine treatment [53]. This is consistent with the present study showing that *F. nucleatum* biofilm exhibited a relatively lower susceptibility to nanoparticle-mediating aPDT, compared to *sanguinis* and *P. gingivalis*. The live/dead analysis not only supplemented the MTT and CFU quantification results, but also enabled the visualization of the perturbations of biofilms caused by aPDT. In summary, all antimicrobial assessments revealed that the photoexcited Fe_3O_4-silane@Ce6/C6 and silane@Ce6/C6 MNPs consistently exhibited much higher antimicrobial potency than that achieved previously. This was demonstrated against both Gram-negative and Gram-positive bacteria, and in both planktonic and biofilm phases.

As a new antimicrobial strategy, aPDT can be an alternative to conventional antibiotic applications in periodontitis treatment. However, over-irradiation may cause tissue injury. Hence, it is necessary to accurately monitor and control the aPDT in real time. Recently, clinical application of fiber optic intravital endoscopic devices made real-time monitoring feasible and realistic [54]. In the present study, C6 was selected as the co-loading molecule, because Ce6 and C6 can be co-excited by the 405 nm wavelength, but C6 would not be excited by 630 nm, and the luminescent intensity of C6 would remain constant. Therefore, the ratio emission of Ce6 and C6 in the nanoparticles can be used to perform accurate monitoring. The green signal of C6 was clear after light irradiation, while the emission from Ce6 (red signal) in the area was still difficult to report because of the consumption of Ce6.

To certify the hypothesis that Fe_3O_4-silane@Ce6/C6 MNPs had the magnetic targeting capability to enable deep penetration into the biofilm, the antibacterial activity via Fe_3O_4-silane@Ce6/C6 MNPs was investigated with or without the use of a magnet. In general, $^1O_2$ can diffuse for approximately 50 nm and will quickly disappear in approximately 3.5 μs following its generation [55]. Hence, the distance of $^1O_2$ diffusion to the bacterial cells is of significant importance for the aPDT activity. Henderson et al. proposed that the $^1O_2$-induced photodamage from porphyrin activation is usually localized to within 0.1 μm of its site of release [56]. The present study suggested that the magnetic targeting effect could result in the photosensitizer molecule to be close to the bacterial surface, thereby facilitating the diffusion of singlet oxygen into the resident bacterial cells. This then helps to completely eliminate the biofilm. Regarding aPDT for periodontitis treatment, the periodontal pockets often possess complicated structures, such as furcations, deep invaginations and concavities, which would impede antibacterial agents to reach the exact site of infection. Therefore, Fe_3O_4-silane@Ce6/C6 MNPs with magnetic targeting ability could magnetically control the aPDT, thus offering a novel and imperative approach for the treatment of recalcitrant and the costly and prevalent periodontal infections.

Besides local administration in the periodontal pocket for periodontitis treatment, the multifunctional MNPs of the present study are promising for treating other bacteria-related oral diseases, such as caries, endodontic infections and periapical diseases [57,58]. Furthermore, dental resins such as composites and bonding agents are widely used as filling materials due to their esthetics and direct-filling capabilities [59–61]. However, such dental materials are challenged with accumulation of more biofilms than other restorative materials, which could result in secondary caries. Recently, efforts were made to develop antibacterial dental resins [62,63]. Further studies should investigate the aPDT functions of Fe_3O_4-silane@Ce6/C6 MNPs for incorporation into resin-based dental materials. For example, the magnetic properties of Fe_3O_4-silane@Ce6/C6 MNPs could benefit the deeper penetration and enhance the bonding strength of dental adhesives. In addition, laser energy at 630 nm could penetrate through the gingival and bone tissues to reach the intended target sites to improve the efficacy of treatments.

Although the multifunctional nanoparticles possessed a strong antibiofilm ability, they showed little selectivity against all bacterial strains in the oral microenvironment (including the benign oral bacterial strain). Further studies should focus on specific targeting of nanoparticles against periodontal pathogens without harming the balance of the oral microenvironment.

5. Conclusions

The present study developed the multifunctional Fe_3O_4-silane@Ce6/C6 nanoparticles by co-loading Ce6 and C6 into the hydrophobic interspace between the octadecyl groups of oleic acid on the surface of Fe_3O_4 and the alkyl chains of silane. The Fe_3O_4-silane@Ce6/C6 nanoparticles exhibited good water-solubility, chemical stability and biocompatibility. The nanoparticles exerted aPDT effect via Ce6, providing strong antibacterial functions against three species of periodontitis-related biofilm for the first time. The Fe_3O_4-silane@Ce6/C6-mediated aPDT had much greater reduction in biofilms than the control groups. Biofilm CFU was reduced by about 4–5 orders of magnitude via Fe_3O_4-silane@Ce6/C6-mediated aPDT, compared to control groups. To avoid over-irradiation, ratio metric emissions of Ce6 and C6 were applied to monitor the aPDT level in real time. The incorporation of Fe_3O_4 in the nanoparticles did not compromise the aPDT efficiency, while providing the magnetic targeting capability. Therefore, the multifactional Fe_3O_4-silane@Ce6/C6 MNPs have great potential for antibacterial treatments in periodontal and other dental applications.

Conflicts of interest

There are no conflicts to declare.

Acknowledgements

We thank Dr. Hongwei Xu from Jilin University for experimental help. This work was supported by National Science Foundation of China81570983 (YZ), 81400487 (LW), 61775080 (BD), International Cooperation Project of Science and Technology Development Jilin Province20180414030GH (YZ), China Postdoctoral Science Foundation2015M581405, 2017T100213 (LW), the 13th Five-Year Plan of the Science Foundation of Education Board of Jilin ProvinceJJKH20180235KJ (LW), and University of Maryland School of Dentistry Seed Grant (HX).

References

[1] G.E. Holde, N. Oscarson, T.A. Trovik, A. Tillberg, B. Jönsson, Periodontitis prevalence and severity in adults: a cross-sectional study in Norwegian circumpolar communities, J. Periodontol. 88 (10) (2017) 1012–1022.
[2] N.J. Kassebaum, E. Bernabé, M. Dahiya, B. Bhandari, C.J.L. Murray, W. Marcenes, Global burden of severe periodontitis in 1990-2010: a systematic review and meta-regression, J. Dent. Res. 93 (11) (2014) 1045–1053.
[3] K. Jepsen, S. Jepsen, Antibiotics/antimicrobials: systemic and local administration in the therapy of mild to moderately advanced periodontitis, Periodontol. 2000 71 (1) (2016) 82–112.
[4] P.A. Adriaens, L.M. Adriaens, Effects of nonsurgical periodontal therapy on hard and soft tissues, Periodontol. 2000 36 (1) (2004) 121–145.
[5] M. Umeda, Y. Takeuchi, K. Noguchi, Y. Huang, G. Koshy, I. Ishikawa, Effects of nonsurgical periodontal therapy on the microbiota, Periodontol. 2000 36 (1) (2004) 98–120.
[6] A. Pfitzner, B.W. Sigusch, V. Albrecht, E. Glockmann, Killing of periodontopathogenic bacteria by photodynamic therapy, J. Periodontol. 75 (10) (2004) 1343–1349.
[7] E.T. Carrera, H.B. Dias, S.C.T. Corbi, R.A.C. Marcantonio, A.C.A. Bernardi, V.S. Bagnato, M.R. Hamblin, A.N.S. Rastelli, The application of antimicrobial photodynamic therapy (aPDT) in dentistry: a critical review, Laser Phys. 26 (12) (2016) 123001.
[8] X. Dai, X. Chen, Y. Zhao, Y. Yu, X. Wei, X. Zhang, C. Li, A water-soluble galactose-decorated cationic photodynamic therapy agent based on BODIPY to selectively eliminate biofilm, Biomacromolecules 19 (1) (2017) 141–149.
[9] M. Wilson, M. Gibson, D. Strahan, W. Harvey, A preliminary evaluation of the use of a redox agent in the treatment of chronic periodontitis, J. Periodontal Res. Suppl. 27 (5) (1992) 522–527.
[10] J. Xu, P. Yang, M. Sun, H. Bi, B. Liu, D. Yang, S. Gai, F. He, J. Lin, Highly emissive dye-sensitized upconversion nanostructure for dual-photosensitizer photodynamic therapy and bioimaging, ACS Nano 11 (4) (2017) 4133–4144.
[11] A. Al-Ahmad, A. Walankiewicz, E. Hellwig, M. Follo, C. Tennert, A. Wittmer, L. Karygianni, Photoinactivation using visible light plus water-filtered infrared-a (vis + wIRA) and chlorine e6 (Ce6) eradicates planktonic periodontal pathogens and subgingival biofilms, Front. Microbiol. 7 (2016) 1900.
[12] P. Müller, B. Guggenheim, P.R. Schmidlin, Efficacy of gasiform ozone and photodynamic therapy on a multispecies oral biofilm in vitro, Eur. J. Oral Sci. 115 (1) (2007) 77–80.
[13] N.S. Soukos, S.E. Mulholland, S.S. Socransky, A.G. Doukas, Photodestruction of human dental plaque bacteria: enhancement of the photodynamic effect by photomechanical waves in an oral biofilm model, Lasers Surg. Med. Suppl. 33 (3) (2010) 161–168.
[14] V.E. Salgado, L.M. Cavalcante, R.R. Moraes, H.B. Davisd, J.L. Ferracaned, L.F. Schneiderc, Degradation of optical and surface properties of resin-based composites with distinct nanoparticle sizes but equivalent surface area, J. Dent. 59 (2017) 48–53.
[15] G.C. Padovani, V.P. Feitosa, S. Sauro, F.R. Tay, G. Durán, A.J. Paula, N. Durán, Advances in dental materials through nanotechnology: facts, perspectives and toxicological aspects, Trends Biotechnol. 33 (11) (2015) 621–636.
[16] L.M. de Freitas, G.M.F. Calixto, M. Chorilli, J.S.M. Giusti, V.S. Bagnato, N.S. Soukos, M.M. Amiji, C.R. Fontana, Polymeric nanoparticle-based photodynamic therapy for chronic periodontitis in vivo, Int. J. Mol. Sci. 17 (5) (2016) 769.
[17] A. Shrestha, M.R. Hamblin, A. Kishen, Photoactivated rose bengal functionalized chitosan nanoparticles produce antibacterial/biofilm activity and stabilize dentin-collagen, Nanomed.: Nanotechnol. Biol. Med. 10 (3) (2014) 491–501.
[18] K.O. Wikene, A.B. Hegge, E. Bruzell, H.H. Tønnesen, Formulation and characterization of lyophilized curcumin solid dispersions for antimicrobial photodynamic therapy (aPDT): studies on curcumin and curcuminoids LII, Drug Dev. Ind. Pharm. 41 (6) (2015) 969–977.
[19] W. Yao, P. Xu, J. Zhao, L. Ling, X. Li, B. Zhang, N. Cheng, Z. Pang, RGD functionalized polymeric nanoparticles targeting periodontitis epithelial cells for the enhanced treatment of periodontitis in dogs, J. Colloid Interface Sci. 458 (2015) 14–21.
[20] Z. Dong, L. Feng, W. Zhu, X. Sun, M. Gao, H. Zhao, Y. Chao, Z. Liu, $CaCO_3$ nanoparticles as an ultra-sensitive tumor-pH-responsive nanoplatform enabling real-time drug release monitoring and cancer combination therapy, Biomaterials 110 (2016) 60–70.
[21] J. Wang, H. Xia, B.B. Xu, L.G. Niu, D. Wu, Q.D. Chen, H.B. Sun, Remote manipulation of microнanomachines containing magnetic nanoparticles, Opt. Lett. 34 (5) (2009) 581–583.
[22] Y. Liu, Z. Li, L. Wu, Z. Wang, X. Wang, Y. Yu, Q. Zhao, F. Luo, MiRNA-125a-5p: a regulator and predictor of Gefitinib's effect on nasopharyngeal carcinoma, Cancer Cell Int. 14 (1) (2014) 24.
[23] L. Wang, X. Xie, S. Imazato, M.D. Weir, M.A. Reynolds, H.H.K. Xu, A protein-repellent and antibacterial nanocomposite for Class-V restorations to inhibit periodontitis-related pathogens, Mater. Sci. Eng. C 67 (2016) 702–710.
[24] E.A.C. Olivo, D. Santos, M.E. de Lima, V.L. dos Santos, R.D. Sinisterra, M.E. Cortés, Antibacterial effect of synthetic peptide LyeTxl and LyeTxl/βCD association compound against planktonic and multispecies biofilms of periodontal pathogens, J. Periodontol. 88 (6) (2017) e88–96.
[25] G. Subbiahdoss, S. Sharifi, D.W. Grijpma, S. Laurent, H.C.V. der Mei, M. Mahmoudi, H.J. Busscher, Magnetic targeting of surface-modified superparamagnetic iron oxide nanoparticles yields antibacterial efficacy against biofilms of gentamicin-resistant staphylococci, Acta Biomater. 8 (6) (2012) 2047–2055.
[26] P. Huang, Z. Li, J. Lin, D. Yang, G. Gao, C. Xu, L. Bao, C. Zhang, K. Wang, H. Song, H. Hu, D. Cui, Photosensitizer-conjugated magnetic nanoparticles for *in vivo* simultaneous magnetofluorescent imaging and targeting therapy, Biomaterials 32 (13) (2011) 3447–3458.
[27] M.T. Mathew, S. Abbey, N.J. Hallab, D.J. Hall, C. Sukotjo, M.A. Wimmer, Influence of pH on the tribocorrosion behavior of CpTi in the oral environment: synergistic interactions of wear and corrosion, J. Biomed. Mater. Res. Part B Appl. Biomater. 100 (6) (2012) 1662–1671.
[28] X. Wang, K. Liu, G. Yang, L. Cheng, L. He, Y. Liu, Y. Li, L. Guo, Z. Liu, Near-infrared

light triggered photodynamic therapy in combination with gene therapy using upconversion nanoparticles for effective cancer cell killing, Nanoscale 6 (15) (2014) 9198–9205.
[29] K. Konopka, T. Goslinski, Photodynamic therapy in dentistry, J. Dent. Res. 86 (8) (2007) 694–707.
[30] N. Kashef, M.R. Hamblin, Can microbial cells develop resistance to oxidative stress in antimicrobial photodynamic inactivation? Drug Resist. Updat. 31 (2017) 31–42.
[31] P. Diogo, C. Fernandes, F. Caramelo, M. Mota, I.M. Miranda, M.A.F. Faustino, M.G.P.M.S. Neves, M.P. Uliana, K.T. de Oliveira, J.M. Santos, T. Gonçalves, Antimicrobial photodynamic therapy against endodontic Enterococcus faecalis and Candida albicans mono and mixed biofilms in the presence of photosensitizers: a comparative study with classical endodontic irrigants, Front. Microbiol. 8 (2017) 498.
[32] L. Misba, S. Zaidi, A.U. Khan, Efficacy of photodynamic therapy against Streptococcus mutans biofilm: Role of singlet oxygen, J. Photochem. Photobiol. B 183 (2018) 16–21.
[33] Z. Zhou, F. Hu, S. Hu, M. Kong, C. Feng, Y. Liu, X. Cheng, Q. Ji, X. Chen, pH-activated nanoparticles with targeting for the treatment of oral plaque biofilm, J. Mater. Chem. B Mater. Biol. Med. 6 (4) (2018) 586–592.
[34] X. Li, M. Gao, K. Xin, L. Zhang, D. Ding, D. Kong, Z. Wang, Y. Shi, F. Kiessling, T. Lammers, J. Cheng, Y. Zhao, Singlet oxygen-responsive micelles for enhanced photodynamic therapy, J. Control. Release 260 (2017) 12–21.
[35] G. Patianna, N.A. Valente, A. D'Addona, S. Andreana, *In vitro* evaluation of controlled-release 14% doxycycline gel for decontamination of machined and sand-blasted acid-etched implants, J. Periodontol. 89 (3) (2018) 325–330.
[36] S.S. Socransky, A.D. Haffajee, M.A. Cugini, C. Smith, R.L. Jr Kent, Microbial complexes in subgingival plaque, J. Clin. Periodontol. 25 (2) (1998) 134–144.
[37] X. Li, K.M. Kolltveit, L. Tronstad, I. Olsen, Systemic diseases caused by oral infection, Clin. Microbiol. Rev. 13 (4) (2000) 547–558.
[38] P.W. Caufield, A.P. Dasanayake, Y. Li, Y. Pan, J. Hsu, J.M. Hardin, Natural history of Streptococcus sanguinis in the oral cavity of infants: evidence for a discrete window of infectivity, Infect. Immun. 68 (7) (2000) 4018–4023.
[39] P.D. Marsh, E. Zaura, Dental biofilm: ecological interactions in health and disease, J. Clin. Periodontol. 44 (S18) (2017) S12–S22.
[40] V. Blanc, S. Isabal, M.C. Sanchez, A. Llama-Palacios, D. Herrera, M. Sanz, R. León, Characterization and application of a flow system for *in vitro* multispecies oral biofilm formation, J. Periodontal Res. Suppl. 49 (3) (2014) 323–332.
[41] H. Rath, S.N. Stumpp, M. Stiesch, Development of a flow chamber system for the reproducible *in vitro* analysis of biofilm formation on implant materials, PLoS One 12 (2) (2017) e0172095.
[42] Q. Guo, Y. Zhao, X. Dai, T. Zhang, Y. Yu, X. Zhang, C. Li, Functional silver nanocomposites as broad-spectrum antimicrobial and biofilm-disrupting agents, ACS Appl. Mater. Inter. 9 (20) (2017) 16834–16847.
[43] X. Dai, X. Chen, Y. Zhao, Y. Yu, X. Wei, X. Zhang, C. Li, A water-soluble galactose-decorated cationic photodynamic therapy agent based on BODIPY to selectively eliminate biofilm, Biomacromolecules. 19 (1) (2017) 141–149.
[44] J.K. Lee, S.H. Park, H.S. Um, S.Y. Lee, B.S. Chang, Comparison of periodontitis-associated oral biofilm formation under dynamic and static conditions, J. Periodontal Implant Sci. 47 (4) (2017) 219–230.
[45] F. Li, M.D. Weir, A.F. Fouad, H.H.K. Xu, Effect of salivary pellicle on antibacterial activity of novel antibacterial dental adhesives using a dental plaque microcosm biofilm model, Dent. Mater. 30 (2) (2014) 182–191.
[46] S.Q. Gong, D.J. Epasinghe, B. Zhou, L.N. Niu, K.A. Kimmerling, F.A. Rueggeberg, C.K.Y. Yiu, J. Mao, D.H. Pashley, F.R. Tay, Effect of water-aging on the antimicrobial activities of an ORMOSIL-containing orthodontic acrylic resin, Acta Biomater. 9 (6) (2013) 6964–6973.
[47] S.V.W. Sutton, R.E. Marquis, Membrane-associated and solubilized ATPases of Streptococcus mutans and Streptococcus sanguis, J. Dent. Res. 66 (6) (1987) 1095–1098.
[48] A. Michaeli, J. Feitelson, Reactivity of singlet oxygen toward amino acids and peptides, Photochem. Photobiol. 59 (3) (1994) 284–289.
[49] S. Tubby, M. Wilson, J.A. Wright, P. Zhang, S.P. Nair, Staphylococcus aureus small colony variants are susceptible to light activated antimicrobial agents, BMC Microbiol. 13 (1) (2013) 201.
[50] D.Y. Gao, X. Ji, J.L. Wang, Y.T. Wang, D.L. Li, Y.B. Liu, K.W. Chang, J.L. Qu, J. Zheng, Z. Yuan, Engineering a protein-based nanoplatform as an antibacterial agent for light activated dual-modal photothermal and photodynamic therapy of infection in both the NIR I and II windows, J. Mater. Chem. B Mater. Biol. Med. 6 (5) (2018) 732–739.
[51] S. Liu, T.H. Zeng, M. Hofmann, E. Burcombe, J. Wei, R. Jiang, J. Kong, Y. Chen, Antibacterial activity of graphite, graphite oxide, graphene oxide, and reduced graphene oxide: membrane and oxidative stress, ACS Nano 5 (9) (2011) 6971–6980.
[52] M.A. Vargas-Reus, K. Memarzadeh, J. Huang, G.G. Ren, R.P. Allaker, Antimicrobial activity of nanoparticulate metal oxides against peri-implantitis pathogens, Int. J. Antimicrob. Agents 40 (2) (2012) 135–139.
[53] Y. Hosaka, A. Saito, R. Maeda, C. Fukaya, S. Morikawa, A. Makino, K. Ishihara, T. Nakagawa, Antibacterial activity of povidone–iodine against an artificial biofilm of Porphyromonas gingivalis and Fusobacterium nucleatum, Arch. Oral Biol. 57 (4) (2012) 364–368.
[54] A. Movila, M. Kajiya, W. Wisitrasameewong, P. Stashenko, S. Vardar-Sengul, M. Hernandez, H.T. Temple, T. Kawai, Intravital endoscopic technology for real-time monitoring of inflammation caused in experimental periodontitis, Immunol. Methods 457 (2018) 26–29.
[55] C. Chui, K. Hiratsuka, A. Aoki, Y. Takeuchi, Y. Abiko, Y. Izumi, Blue LED inhibits the growth of Porphyromonas gingivalis by suppressing the expression of genes associated with DNA replication and cell division, Lasers Surg. Med. Suppl. 44 (10) (2012) 856–864.
[56] B.W. Henderson, T.J. Dougherty, How does photodynamic therapy work? Photochem. Photobiol. 55 (1) (1992) 145–157.
[57] D. Khvostenko, T.J. Hilton, J.L. Ferracane, J.C. Mitchell, J.J. Kruzic, Bioactive glass fillers reduce bacterial penetration into marginal gaps for composite restorations, Dent. Mater. 32 (1) (2016) 73–81.
[58] J.L. Roberts, J.Y. Maillard, R.J. Waddington, S.P. Denyer, C.D. Lynch, A.J. Sloan, Development of an ex vivo coculture system to model pulpal infection by Streptococcus anginosus group bacteria, J. Endodont. 39 (1) (2013) 49–56.
[59] C.D. Lynch, N.J. Opdam, R. Hickel, P.A. Brunton, S. Gurgan, A. Kakaboura, A.C. Shearer, G. Vanherle, N.H.F. Wilson, Guidance on posterior resin composites: academy of operative dentistry-European section, J. Dent. 42 (4) (2014) 377–383.
[60] J.L. Ferracane, Resin composite—state of the art, Dent. Mater. 27 (1) (2011) 29–38.
[61] N.J.M. Opdam, K. Collares, R. Hickel, S.C. Bayne, B.A. Loomans, M.S. Cenci, C.D. Lynch, M.B. Correa, F. Demarco, F. Schwendicke, N.H.F. Wilson, Clinical studies in restorative dentistry: new directions and new demands, Dent. Mater. 34 (1) (2018) 1–12.
[62] Y. Liu, L. Zhang, L. Niu, T. Yu, H.H.K. Xu, M.D. Weir, T.W. Oates, F.R. Tay, J. Chen, Antibacterial and remineralizing orthodontic adhesive containing quaternary ammonium resin monomer and amorphous calcium phosphate nanoparticles, J. Dent. 72 (1) (2018) 53–63.
[63] S. Imazato, M. Torii, Y. Tsuchitani, J.F. McCabe, R.R.B. Russell, Incorporation of bacterial inhibitor into resin composite, J. Dent. Res. 73 (8) (1994) 1437–1443.